JACS
JOURNAL OF THE AMERICAN CHEMICAL SOCIETY
Article
pubs.acs.org/JACS

Exceptional Hydrophobicity of a Large-Pore Metal–Organic Zeolite

Chun-Ting He,[†] Lu Jiang,[†] Zi-Ming Ye,[†] Rajamani Krishna,[‡] Zhen-Song Zhong,[†] Pei-Qin Liao,[†] Jianqiao Xu,[†] Gangfeng Ouyang,[†] Jie-Peng Zhang,*[,†] and Xiao-Ming Chen[†]

[†]MOE Key Laboratory of Bioinorganic and Synthetic Chemistry, School of Chemistry and Chemical Engineering, Sun Yat-Sen University, Guangzhou 510275, China

[‡]Van't Hoff Institute for Molecular Sciences, University of Amsterdam, Science Park 904, 1098 XH Amsterdam, The Netherlands

Supporting Information

ABSTRACT: Porous materials combining high hydrophobicity, large surface area, as well as large and uniform pore size are very useful but rare. The nanoporous zeolitic metal azolate framework, RHO-$[Zn(eim)_2]$ (MAF-6, Heim = 2-ethylimidazole), is an attractive candidate but thought to be unobtainable/unstable. In this work, the supramolecular isomerism of $[Zn(eim)_2]$ is thoroughly studied using a rapid solution mixing reaction of $[Zn(NH_3)_4](OH)_2$ and Heim, which enables MAF-6 with high crystallinity, purity, and thermal/chemical stabilities to be synthesized in large quantity. Gas and vapor adsorption isotherms, gas chromatography, and water contact angle measurements, as well as transient breakthrough and molecular dynamics simulations show that MAF-6 exhibits large surface area (langmuir surface area 1695 $m^2\ g^{-1}$), pore volume (0.61 $cm^3\ g^{-1}$), pore size (d = 18.4 Å), and aperture size (d = 7.6 Å) with high hydrophobicity on both the internal pore and external crystal surfaces. It can barely adsorb water or be wetted by water (contact angle 143°) but readily adsorb large amounts of organic molecules including methanol, ethanol, mesitylene, adamantane, C6–C10 hydrocarbons, xylene isomers, and saturated/unsaturated analogues such as benzene/cyclohexene/cyclohexane or styrene/ethylbenzene. It can also separate these organic molecules from each other as well as from water by preferential adsorption/retention of those having higher hydrophobicity, lipophilicity, or oil/water partition coefficient. These properties are very different with other porous materials such as SOD-$[Zn(mim)_2]$ (Hmim = 2-methylimidazole, MAF-4/ZIF-8) with a hydrophobic pore surface but a hydrophilic crystal surface and small aperture size.

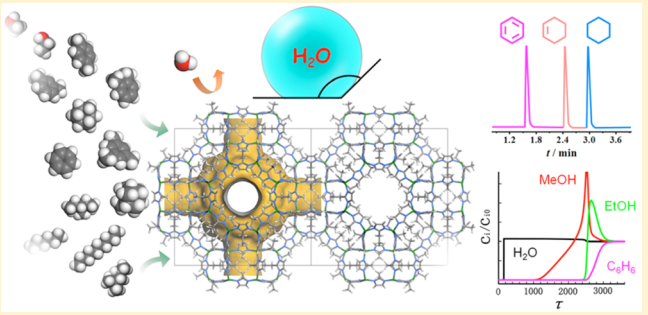

INTRODUCTION

Controlling the surface properties of solids is of paramount importance for a wide range of applications.[1] Highly hydrophobic materials, especially those with high surface areas, are particularly useful for oil/water separation, organic-pollutant enrichment, chromatography analysis, and so on,[2] but they are relatively rare and difficult to design/synthesize because hydrophilic components and defects are generally required and/or unavoidable on the internal pore and external particle surfaces. For example, depending on the synthetic methods, surface heterogeneity (such as oxygen groups and residue metals) and pore size distribution of activated carbons vary a lot, significantly influencing their adsorption and separation performances. The surface heterogeneity and pore size distribution can be largely reduced in crystalline adsorbents with ordered/periodic structures.[1d] A typical example is the pure silica zeolites, such as Silicalite-1, albeit the pore sizes of these inorganic crystals are very small.

Porous coordination polymers (PCPs) or metal–organic frameworks (MOFs) have attracted much attention for their highly ordered, diversified, and designable structures.[3] PCPs with a highly hydrophobic pore surface are rare[4] because it is difficult to control the coordination and guest-interacting behavior of the donor atoms (mostly carboxylate oxygen) of conventional organic ligands, although the hydrophobicity can be improved by using organic ligands with hydrophobic groups (such as aryl, methyl, and ethyl). PCPs with hydrophobic external crystal surfaces are even more scarce[5] because they are always terminated by hydrophilic defects (unsaturated coordination sites), especially for three-dimensional coordination networks, regardless of the hydrophilic/hydrophobic nature of the ligand backbone.

By virtue of the simple/controllable coordination behavior of azolate ligands, such as imidazolate derivatives, the pore surface hydrophilicity/hydrophobicity of metal azolate frameworks (MAFs) could be more easily designed.[6] Based on the relatively long bridging length of the imidazolate ring compared to that of the oxygen atom, the pore sizes of zeolitic MAFs[4f,7] can be much larger than for the inorganic prototypes,[8] which are attractive for adsorption/separation of large organic molecules. Nevertheless, inexpensive and nontoxic building blocks for

Received: April 10, 2015
Published: May 18, 2015

DOI: 10.1021/jacs.5b03727
J. Am. Chem. Soc. 2015, 137, 7217–7223

zeolitic MAFs are very limited due to the strict requirement of the coordination geometries of metal ions and imidazolate-like ligands.[9]

SOD-[Zn(mim)$_2$] (MAF-4 or ZIF-8,[9b,c] Hmim = 2-methylimidazole) is one of the most studied PCPs attributable to its exceptional stability, high porosity, facile/diversified preparation methods, and inexpensive/nontoxic components. Similarly, [Zn(bim)$_2$] (MAF-3 or ZIF-7,[9a,c] Hbim = benzimidazole) has also attracted intensive attention.[10] However, the extremely small apertures of MAF-3 and MAF-4, which have diameters of 2.9 and 3.2 Å, respectively, limit their adsorption/separation of many molecules with larger molecular sizes.[11] In this context, isomeric ANA-[Zn(eim)$_2$] (MAF-5, Heim = 2-ethylimidazolate) and RHO-[Zn(eim)$_2$] (MAF-6)[9b] with larger channel sizes should be attractive. Indeed, MAF-5 has an adsorption affinity for benzene derivatives that is higher than that for MAF-4 because of its larger aperture size (4.0 × 5.8 Å^2), and longer alkyl groups fit better in these large hydrophobic guests, although with a small pore volume.[12]

As defined by its RHO framework topology and ligand structure (Figure 1), the crystal structure of MAF-6 possesses a

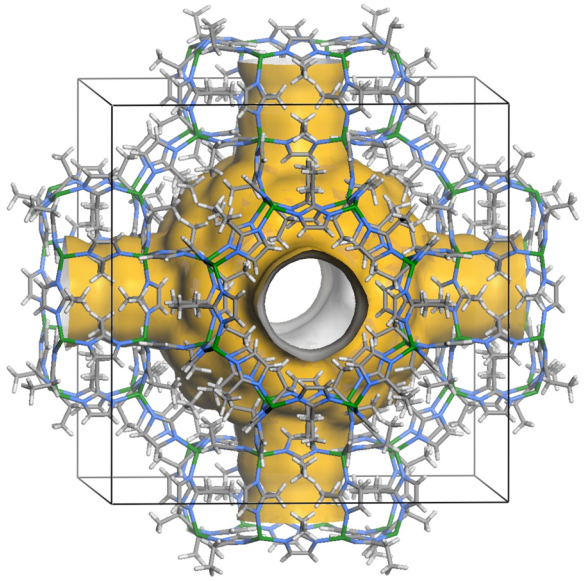

Figure 1. Perspective view of the coordination framework and pore surface structures of MAF-6 (Zn green, N blue, C gray, H white, pore surface yellow/gray, unit-cell edges black).

three-dimensional ethyl-lined hydrophobic pore system with very large cavities (d = 18.1 Å) and large apertures (d = 7.6 Å), as well as a relatively large pore volume (0.63 cm^3 g^{-1}, Supporting Information Table S1). While a few RHO-type PCPs have been reported, they possess either a hydrophilic pore surface or a very small aperture size because of the presence of carboxylate or bulky groups such as a phenyl ring.[7a,b,13] In addition, they are mostly composed of toxic and/or expensive components such as Cd(II), In(III), 2-nitroimidazolate, etc.[7a,c,13,14] Unfortunately, as a rare structure combining large and ordered pores, high hydrophobicity, low toxicity, and low cost, MAF-6 was originally discovered as a minor byproduct of its isomer MAF-5 in the liquid diffusion reaction, preventing investigation of its properties.[9b] Later, Friščić et al. found that MAF-5 and MAF-6 could be synthesized by ion- and liquid-assisted ball milling of ZnO and Heim. However, the obtained materials are of low crystallinity and impurity, which easily transform into the nonporous isomer **qtz**-[Zn(eim)$_2$] (MAF-32) in very short time (<60 min).[15] Herein, we report an efficient method for the rapid/large-scale synthesis of high-quality MAF-6. More importantly, this *new* material couples exceptional hydrophobicity (on both the internal pore and external crystal surfaces) with large pore/aperture size and surface area, which is useful for separation/enrichment applications dealing with water and a large variety of organic molecules.

RESULTS AND DISCUSSION

Controlling Supramolecular Isomerism. The rapid solution mixing of aqueous ammonia solution of ZnO/Zn(OH)$_2$ and methanol solution of an azole ligand is an efficient synthetic method for MAFs.[6] Upon addition of hydrophobic templates or not, we have selectively synthesized MAF-5 and MAF-32 in bulk quantities, respectively.[12] These results inspired us to further study and control the crystallization of Zn(II) 2-ethylimidazolate isomers,[16] by varying the template, feeding order, and concentration of reactants.

First, as a conventional feeding order,[12] the Heim solution was fast added into the [Zn(NH$_3$)$_4$](OH)$_2$ solution premixed with different amounts of a hydrophobic template of benzene or cyclohexane (Scheme 1). White microcrystalline powders

Scheme 1. Controlling Supramolecular Isomerism of Zn(II) 2-Ethylimidazolate by Feeding Order and Template Concentration

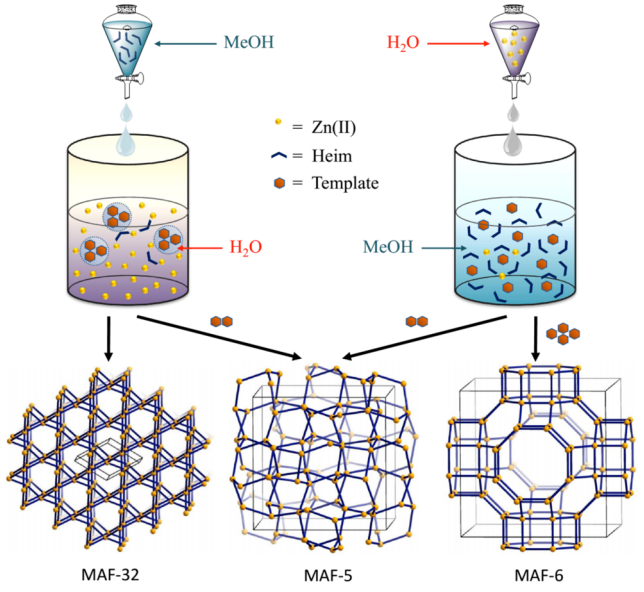

were obtained and identified by powder X-ray diffraction (PXRD). When the template concentration increased gradually, the obtained product varied from pure MAF-32, mixtures of MAF-32 and MAF-5, pure MAF-5, and finally to mixtures of MAF-5 and MAF-6. However, further increase of the template concentration did not produce pure MAF-6 (Figure 2a). These results demonstrated that benzene/cyclohexane can be used as a template for MAF-5 and MAF-6, and high template concentration is favorable but not enough for MAF-6. If the reaction mixtures were further stirred for 3 days, all products transformed to pure MAF-32 (Figure 2a), indicating that MAF-

DOI: 10.1021/jacs.5b03727
J. Am. Chem. Soc. 2015, 137, 7217−7223

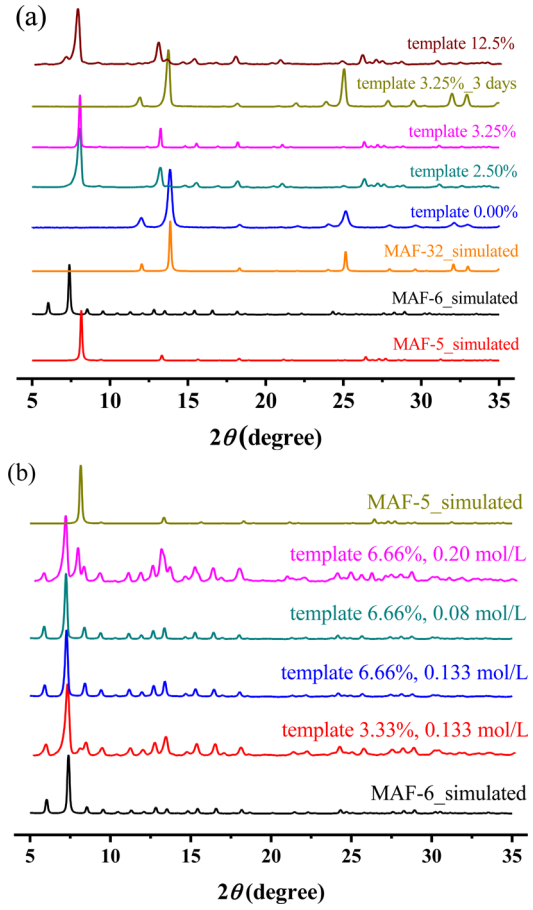

Figure 2. PXRD patterns of the products obtained by adding (a) methanol solution of Heim into a concentrated aqueous ammonia solution of $Zn(OH)_2$ premixed with different concentrations of template or (b) concentrated aqueous ammonia solution of $Zn(OH)_2$ into different concentrations of methanol solution of Heim premixed with different concentrations of template.

5/MAF-6 and MAF-32 are kinetically and thermodynamically favored phases, respectively.

Obviously, high template concentration is favorable for yielding MAF-6, but aqueous ammonia poorly dissolves the hydrophobic templates. Therefore, we premixed the template with the methanol solution of Heim and also changed the feeding order of the reaction, so that the reaction can start and occur mainly in methanol with a high concentration of template. Without a template, the MAF-5/MAF-6 mixture, pure MAF-5, and the MAF-5/MAF-32 mixture were obtained from low (≤0.13 mol/L) to high (≥0.20 mol/L) ligand concentrations, respectively (Figure S1), indicating that the solvent methanol may also serve as a hydrophobic template for MAF-5 and MAF-6, but pure MAF-6 can be barely obtained in this way. While the Heim solution with relatively low concentration (0.08−0.13 mol/L) was premixed with enough cyclohexane (6.66%, v/v), pure MAF-6 was finally obtained. With less cyclohexane and/or higher ligand concentration (0.20 mol/L), the products were still mixtures of MAF-6 and MAF-5 (Figure 2b). Additionally, MAF-6 can be similarly prepared in other polar organic solvents such as ethanol (Figure S2).

According to the above results, the main difference between the syntheses of MAF-5 and MAF-6 was the feeding order. MAF-6 was obtained by adding the metal ion solution into the ligand solution premixed with the hydrophobic template. Obviously, such a feeding order can furnish higher efficiency of the template effect because the reaction happened in the presence of high-concentration hydrophobic templates. Besides, the lower Heim concentration can also improve the effect of template as the ratio of template/Heim will increase in the reaction system. It is obvious that the lower the template/Heim ratio, the more possibility there is to produce MAF-5 or MAF-32, which rely less on the template (Scheme 1). The fact that MAF-6 needs more amounts of template and lower ligand concentration than does MAF-5 might be attributed to the higher porosity of MAF-6.

Stability and Porosity. A thermogravimetric curve of MAF-6 obtained by the above-mentioned method indicated no weight loss below 400 °C (Figure S3). PXRD showed that the original crystallinity could be retained even after being heated at 400 °C in a nitrogen atmosphere for 1 h or immersed in methanol, benzene, and even water at room temperature for at least 3 days (Figure S4). Such thermal and chemical stabilities are relatively high among PCPs.[17] The poor stability of MAF-6 synthesized by the ion-/liquid-assisted ball milling method reported in the literature might be ascribed to their poor crystallinity and presence of ammonium salts.[15]

A N_2 sorption isotherm of MAF-6 measured at 77 K revealed a langmuir surface area of 1695 $m^2\ g^{-1}$ and a Brunauer−Emmett−Teller surface area of 1343 $m^2\ g^{-1}$, as well as a pore volume of 0.61 $cm^3\ g^{-1}$ (Figure 3a). The pore size distribution

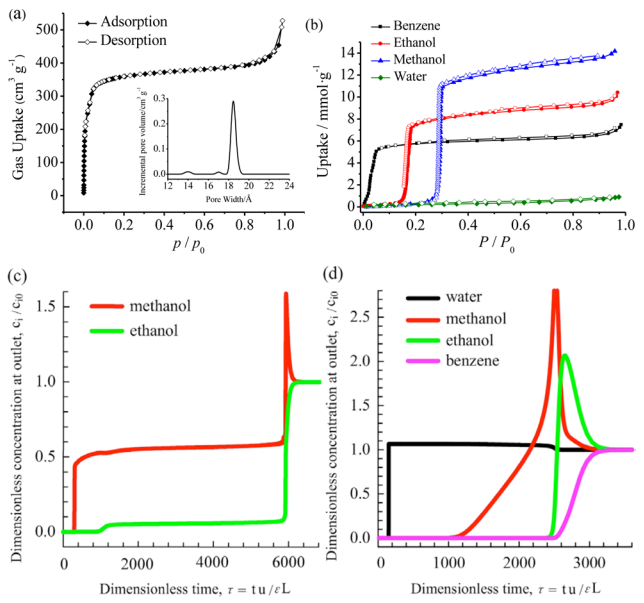

Figure 3. (a) Isotherm for N_2 adsorption at 77 K and pore size distribution (inset) of MAF-6 and (b) benzene, ethanol, methanol, and water vapor adsorption isotherms measured at 298 K. Transient breakthrough calculations for (c) a 50/50 methanol/ethanol mixture at 10 kPa and (d) an 85/5/5/5 water/methanol/ethanol/benzene mixture at 100 kPa in a packed bed of MAF-6 at 298 K.

profile was calculated by the density functional theory model using the isotherm, which showed one very sharp peak centered at 18.4 Å. These values are consistent with those calculated from the crystal structure of MAF-6, indicating the good crystallinity and purity of the sample synthesized in this work. The pore size and surface area of MAF-6 are much larger than those of the most open inorganic zeolites[8] as well as most zeolitic PCPs.[7b]

DOI: 10.1021/jacs.5b03727
J. Am. Chem. Soc. 2015, 137, 7217−7223

Pore Surface Hydrophobicity. To study the pore surface characteristics of MAF-6, water, methanol, ethanol, and benzene sorption isotherms were measured at room temperature. As shown in Figure 3b, MAF-6 can adsorb large amounts of benzene, ethanol, and methanol, with saturation uptakes of 6.36, 9.15, and 13.27 mmol g^{-1} and corresponding pore volumes of 0.57, 0.53, and 0.54 cm^3 g^{-1}, respectively. These pore volumes are slightly smaller than the theoretical one empirically calculated from its crystal structure (0.63 cm^3 g^{-1}), due to the fact that nondense packing of actual molecules with specific shapes cannot fully utilize all spaces. The sorption isotherm of benzene shows a type IV characteristic, while those of ethanol and methanol can be described as type V (S-shaped). The abrupt increases of uptakes of benzene, ethanol, and methanol started at $P/P_0 \approx 0.02$, 0.14, and 0.26, respectively (Figure 3b). It is worth pointing out that the difference of the inflection pressures between methanol and ethanol sorption in MAF-6 (0.26−0.14 = 0.12) is much larger than those in the most studied hydrophobic PCPs such as MAF-4 (0.10−0.05 = 0.05) and ZIF-71 (0.20−0.12 = 0.08).[18] More remarkably, MAF-6 can barely adsorb water with just 0.90 mmol g^{-1} uptake at $P/P_0 = 0.97$.[4c,9b] The very different sorption isotherms for these typical solvents confirm the hydrophobic nature of the pore surface of MAF-6, which shows higher affinity for the more hydrophobic adsorbates.

We further carried out breakthrough simulations for a fixed-bed adsorber packed with MAF-6 through the established methodology described in earlier publications (Figures S5 and S6).[19] Using a 50/50 methanol/ethanol mixture, it can be seen that methanol is rejected into the bulk fluid phase and ethanol is preferentially adsorbed (Figure 3c). Further, for an 85/5/5/5 water/methanol/ethanol/benzene mixture, water can be rejected in the bulk fluid phase and the polar/organic compounds can be selectively adsorbed. The elution order followed the polarity of the solvents, consistent with the order of their isotherm inflection pressures (Figure 3d). These results suggest MAF-6 as a promising candidate for applications on organic/water, alcohol/water, and especially methanol−ethanol separations, which are highly demanded yet very difficult to obtain.[18,20]

Crystal Surface Hydrophobicity. Interestingly, a water droplet can maintain its shape and roll on the powders of MAF-6 (Figure S7), and MAF-6 powders can float on the water surface. This character coupled with its large hydrophobic internal pore makes MAF-6 useful for extracting organic liquids/solids floating on or dissolved/dispersed in water, even for those with molecular sizes as large as cyclohexane (5.0 × 6.6 × 7.2 $Å^3$), mesitylene (4.1 × 8.3 × 8.6 $Å^3$), and adamantane (7.6 × 7.6 × 7.6 $Å^3$). Also, importantly, after large amounts of these guests are loaded, MAF-6 can still float on water (Figure 4 and Figures S8 and S9), indicating the crucial role of the high hydrophobicity of the external surface instead of its low crystal density. In contrast, although MAF-4 can also float on water due to its low framework density, it can hardly adsorb the above molecules because of its rather small pore apertures (Figure S10).[9b,11a]

To compare the external, crystal, or particle surface properties of MAF-6 with those of its analogues MAF-4 and MAF-5, we tested their water contact angles. Interestingly, the surface of MAF-6 is highly hydrophobic with a large contact angle of 143 ± 1°, while MAF-5, which contains the same chemical components as MAF-6, is absolutely hydrophilic with a contact angle of 0° (Figure 5a). Further, MAF-4, well-known as a hydrophobic adsorbent,[9d,12] also exhibited a wettable crystal surface with a contact angle of 0° (Figure S11), which has been observed elsewhere and can be ascribed to the defects as well as hydrophilic groups on the crystal surface.[21]

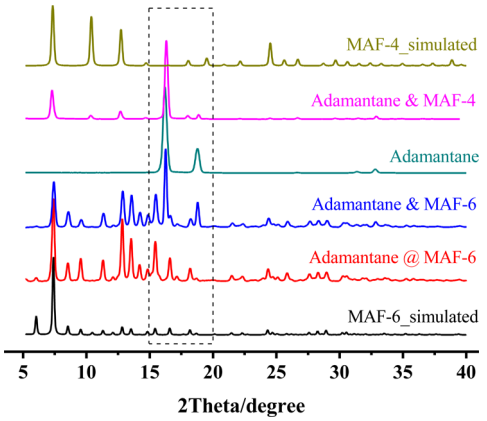

Figure 4. PXRD patterns of MAF-6 or MAF-4 with adamantane before (adamantane and MAF-6) and after being stirred in water (adamantane@MAF-6, adamantane and MAF-4).

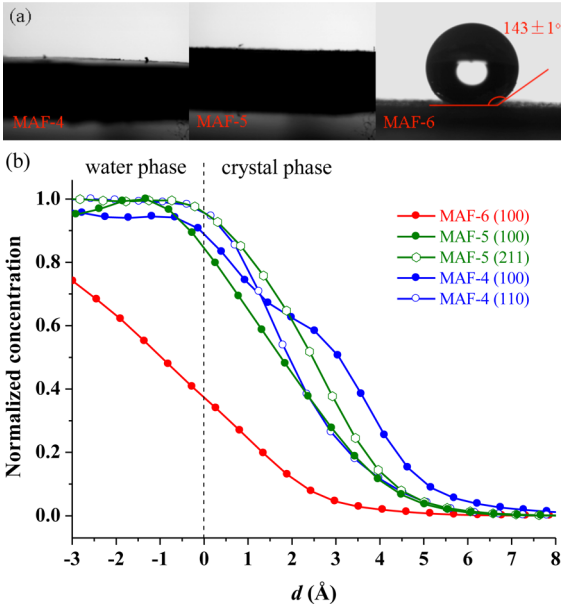

Figure 5. (a) Contact angle images after water droplets balanced on the powders and (b) water concentration distribution (pure water = 1.0) near the crystal surfaces of MAF-4, MAF-5, and MAF-6.

To further explicate such distinctly different crystal surface properties among these MAFs, we simulated their interactions with water molecules. According to their crystal morphologies (Figure S12),[22] we selected the favorite crystal surfaces, that is, (100) and (110) for MAF-4, (100) and (211) for MAF-5, and (100) for MAF-6, as the target models. It has been demonstrated that the unsaturated metal sites on the crystal surfaces were terminated by hydroxyl and/or bicarbonate groups,[23] and for convenience, we adopted hydroxyl groups in all simulations. A layer of water molecules with a density of 1.0 g cm^{-3} was put onto each target crystal surface, and the structure of the water−crystal surface system was simulated by molecular dynamics (MD). The results showed that water molecules are much more repulsive to MAF-6 with concentrations of just 0.38 g cm^{-3} on the studied crystal

DOI: 10.1021/jacs.5b03727
J. Am. Chem. Soc. 2015, 137, 7217−7223

surface. However, water tends to wet the crystal surfaces of MAF-4 and MAF-5 with a concentration >0.85 g cm^{-3} on all the studied crystal surfaces (Figures 5b and S13), which is in accord with the experimental contact angles.

As shown in Figure 6, it is obvious that the (100) crystal surface of MAF-6 contains large basins that originated from its nearly mesoporous cavities, on which there is no incomplete coordination site. In other words, the much higher hydrophobicity of MAF-6, compared with MAF-4 and MAF-5, may arise from its highly corrugated crystal surface on the nanometer scale,[5c] which was similar to the lotus effect on the mesoscopic scale.

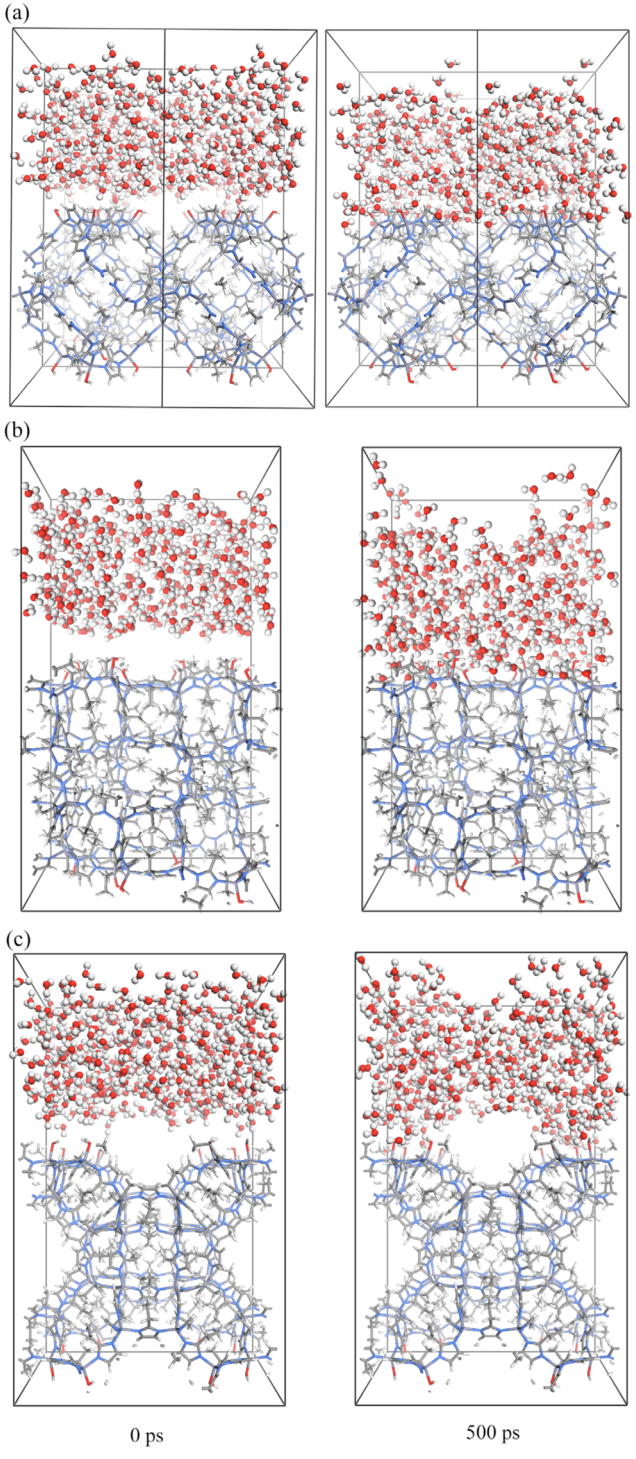

Figure 6. Snapshots of water−crystal surface systems for the (100) crystal surfaces of (a) MAF-4, (b) MAF-5, and (c) MAF-6 obtained from the MD simulations (left, initial configurations at 0 ps; right, optimized configurations after 500 ps).

Sieving Behavior in Gas Chromatography. To test the molecular sieving property of MAF-6 for hydrocarbons such as alkanes and benzene homologues, a gas chromatography (GC) capillary column was fabricated by coating microcrystalline MAF-6 on the inner surface of a quartz capillary. For all groups of analytes, the column exhibited good selectivity, resolution, and precision (Figures S14 and S15 and Table S2), which indicated good quality of the MAF-6 sample and column, as well as excellent performance of the MAF-6 material. Concretely, linear C6−C10 alkanes with a gradual increase of chain length are well-separated on the column following their very different boiling points, giving high selectivities of 2.6−26 (Figure 7a). It has been shown that the aperture size of PCP is important for GC separation of linear alkanes. For example, the capillary column coated by MAF-3 did not offer a baseline separation of linear alkanes, while that coated by MAF-4 achieved good selectivities of 1.4−4.3 for C6−C10 linear alkanes.[11a] The higher selectivities of MAF-6 compared with those of MAF-4 indicated that the stationary phase with larger pore/aperture size and surface area can interact more efficiently with the flowing analytes.

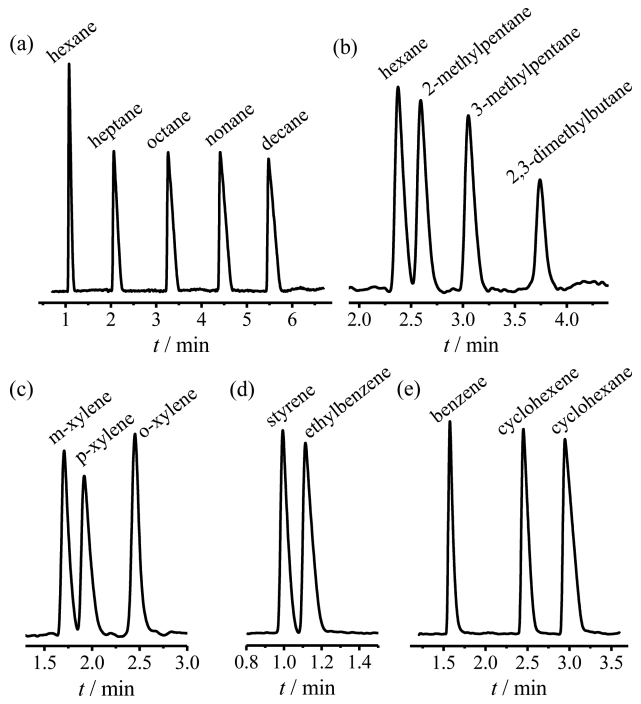

Figure 7. Chromatograms on the MAF-6-coated capillary for GC separation of (a) linear alkanes, (b) hexane and its branched isomers, (c) xylene isomers, (d) styrene and ethylbenzene, and (e) benzene, cyclohexene, and cyclohexane.

Due to the large aperture size of MAF-6, the column can well separate the branched C6 alkane isomers (Figure 7b), which is industrially important and difficult.[24] In contrast, MAF-4 could not separate branched alkanes with a molecular diameter >5.4 Å (such as 2,3-dimethylbutane/2-methylpentane) because they could not pass the narrow pore windows.[11a] It is noteworthy that hexane and 2,3-dimethylbutane possess the shortest and

DOI: 10.1021/jacs.5b03727
J. Am. Chem. Soc. 2015, 137, 7217−7223

longest retention time in the MAF-6 capillary, but they have the highest and lowest boiling points among the four isomers, respectively. This phenomenon is in contrast with that observed for conventional GC columns[24a] but consistent with the hydrophobic selectivity of MAF-6. Actually, the retention times of C6 alkane isomers are in contrast with their average polarizability calculated from time-dependent density functional theory, that is, hexane (85.27) > 2-methylpentane (80.12) > 3-methylpentane (79.91) > 2,3-dimethylbutane (74.63).

Because of the very similar boiling points and molecular shapes of xylene isomers, the most general commercial nonpolar capillary column, HP-5MS, does not get any separation of *p*-xylene and *m*-xylene. Although many stationary phases have been developed for GC separation of xylene isomers, they always need long analysis time[25] and/or temperature programming.[26] The MAF-6 column achieved a very good separation of all three isomers within 2.5 min without the need for temperature programming (Figure 7c), which had not been achieved by other PCPs including UIO-66 and HKUST-1.[24a,27] It was interesting that *p*-xylene eluted after *m*-xylene on the MAF-6-coated capillary column, which is contrast with that on ordinary stationary phases such as poly(ethylene glycol) and MIL-101.[28] Obviously, the polarity of *m*-xylene (dipole moment = 0.36 D, polarizability = 14.2 cm^3) is higher than that for *p*-xylene (dipole moment = 0 D, polarizability = 13.7 cm^3). Therefore, hydrophobic MAF-6 has a stronger interaction with the less polar isomer *p*-xylene. Such abnormal selectivity for *p*-xylene and *m*-xylene has been only observed in a few examples, such as an HPLC column packed with MIL-47.[29]

The hydrophobic characteristic of MAF-6 was further confirmed by the separation of the two groups of saturated/unsaturated analogues, in which the retention times follow ethylbenzene > styrene and cyclohexane > cyclohexene > benzene, although their boiling point sequences are reversed (Figure 7d,e). Again, this phenomenon has not been observed for other PCP-based stationary phases, such as MIL-101(Cr) and amino-MIL-53(Al)[30] because common porous materials interact stronger with the unsaturated analogues, which are easier to be polarized. Obviously, the MAF-6 column has stronger interaction with lipophilic analytes (log $P_{oct/wat}$: ethylbenzene (3.2) > styrene (2.8) and cyclohexane (3.6) > cyclohexene (2.9) > benzene (2.2); see Table S3). Moreover, the adsorption enthalpies calculated from the van't Hoff plots of retention factors measured at different separation temperatures (Figure S16) were consistent with the elution sequence of the tested hydrocarbons (Table S4).

CONCLUSION

In summary, by an in-depth study of the surpramolecular isomerism of Zn(II) 2-ethylimidazolate, we achieved the bulk synthesis of high-quality MAF-6 with high purity and crystallinity and thermal/chemical stability. Based on its unique RHO topology, this material possesses large surface area, pore volume, pore size, and aperture size, as demonstrated by gas, vapor, liquid, and solid adsorption experiments. More importantly, it exhibits exceptional hydrophobicity on both the internal pore and the external crystal surfaces, which originate from its ethyl-lined pore surface and nanoscaled corrugation of the crystal surface. As a consequence, it can separate organic molecules, such as alcohol and hydrocarbons, with molecular sizes ranging from methanol to C6 alkane isomers, xylene isomers, mesitylene, and adamantane, from each other and especially from water, by preferential adsorption/retention of the low-polarity guests, in a variety of application environments. These results suggest that MAF-6, an unusually large-pore and hydrophobic adsorbent consisting of cheap and nontoxic building blocks, can serve as a promising candidate for sorption and separation applications.

ASSOCIATED CONTENT

Supporting Information

Experimental procedures, thermogravimetric curves, PXRD patterns, additional GC analysis data, computational modeling details. The Supporting Information is available free of charge on the ACS Publications website at DOI: 10.1021/jacs.5b03727.

AUTHOR INFORMATION

Corresponding Author

*zhangjp7@mail.sysu.edu.cn

Notes

The authors declare no competing financial interest.

ACKNOWLEDGMENTS

This work was supported by the "973 Project" (2014CB845602 and 2012CB821706) and NSFC (21225105, 21290173, and 21473260).

REFERENCES

(1) (a) Sun, T.; Feng, L.; Gao, X.; Jiang, L. *Acc. Chem. Res.* **2006**, *39*, 487. (b) Lee, H.; Dellatore, S. M.; Miller, W. M.; Messersmith, P. B. *Science* **2007**, *318*, 426. (c) Chu, Z.; Seeger, S. *Chem. Soc. Rev.* **2014**, *43*, 2784. (d) McGuire, C. V.; Forgan, R. S. *Chem. Commun.* **2015**, *51*, 5199. (e) Guo, Y.; Xu, K.; Wu, C.; Zhao, J.; Xie, Y. *Chem. Soc. Rev.* **2015**, *44*, 637.

(2) (a) Montoro, C.; Linares, F.; Quartapelle Procopio, E.; Senkovska, I.; Kaskel, S.; Galli, S.; Masciocchi, N.; Barea, E.; Navarro, J. A. R. *J. Am. Chem. Soc.* **2011**, *133*, 11888. (b) Gu, Z.-Y.; Yang, C.-X.; Chang, N.; Yan, X.-P. *Acc. Chem. Res.* **2012**, *45*, 734. (c) He, C.-T.; Tian, J.-Y.; Liu, S.-Y.; Ouyang, G.; Zhang, J.-P.; Chen, X.-M. *Chem. Sci.* **2013**, *4*, 351. (d) Gao, X.; Xu, L.-P.; Xue, Z.; Feng, L.; Peng, J.; Wen, Y.; Wang, S.; Zhang, X. *Adv. Mater.* **2014**, *26*, 1771. (e) Wang, B.; Liang, W.; Guo, Z.; Liu, W. *Chem. Soc. Rev.* **2015**, *44*, 336.

(3) (a) Cohen, S. M. *Chem. Sci.* **2010**, *1*, 32. (b) He, C.-T.; Liao, P.-Q.; Zhou, D.-D.; Wang, B.-Y.; Zhang, W.-X.; Zhang, J.-P.; Chen, X.-M. *Chem. Sci.* **2014**, *5*, 4755. (c) Yuan, S.; Lu, W.; Chen, Y.-P.; Zhang, Q.; Liu, T.-F.; Feng, D.; Wang, X.; Qin, J.; Zhou, H.-C. *J. Am. Chem. Soc.* **2015**, *137*, 3177.

(4) (a) Pan, L.; Parker, B.; Huang, X.; Olson, D. H.; Lee, L. J. *J. Am. Chem. Soc.* **2006**, *128*, 4180. (b) Horike, S.; Tanaka, D.; Nakagawa, K.; Kitagawa, S. *Chem. Commun.* **2007**, 3395. (c) Zhang, J.-P.; Chen, X.-M. *J. Am. Chem. Soc.* **2008**, *130*, 6010. (d) Yang, C.; Kaipa, U.; Mather, Q. Z.; Wang, X.; Nesterov, V.; Venero, A. F.; Omary, M. A. *J. Am. Chem. Soc.* **2011**, *133*, 18094. (e) Taylor, J. M.; Vaidhyanathan, R.; Iremonger, S. S.; Shimizu, G. K. H. *J. Am. Chem. Soc.* **2012**, *134*, 14338. (f) Nguyen, N. T. T.; Furukawa, H.; Gándara, F.; Nguyen, H. T.; Cordova, K. E.; Yaghi, O. M. *Angew. Chem., Int. Ed.* **2014**, *53*, 10645.

(5) (a) Nguyen, J. G.; Cohen, S. M. *J. Am. Chem. Soc.* **2010**, *132*, 4560. (b) Chen, T.-H.; Popov, I.; Zenasni, O.; Daugulis, O.; Miljanic, O. S. *Chem. Commun.* **2013**, *49*, 6846. (c) Rao, K. P.; Higuchi, M.; Sumida, K.; Furukawa, S.; Duan, J.; Kitagawa, S. *Angew. Chem., Int. Ed.* **2014**, *53*, 8225.

(6) Zhang, J.-P.; Zhang, Y.-B.; Lin, J.-B.; Chen, X.-M. *Chem. Rev.* **2012**, *112*, 1001.

(7) (a) Liu, Y.; Kravtsov, V. C.; Larsen, R.; Eddaoudi, M. *Chem. Commun.* **2006**, 1488. (b) Phan, A.; Doonan, C. J.; Uribe-Romo, F. J.;

DOI: 10.1021/jacs.5b03727
J. Am. Chem. Soc. 2015, 137, 7217−7223

Knobler, C. B.; O'Keeffe, M.; Yaghi, O. M. *Acc. Chem. Res.* **2010**, *43*, 58. (c) Kahr, J.; Mowat, J. P. S.; Slawin, A. M. Z.; Morris, R. E.; Fairen-Jimenez, D.; Wright, P. A. *Chem. Commun.* **2012**, *48*, 6690.
(8) Li, Y.; Yu, J. *Chem. Rev.* **2014**, *114*, 7268.
(9) (a) Huang, X.-C.; Zhang, J.-P.; Chen, X.-M. *Chin. Sci. Bull.* **2003**, *48*, 1531. (b) Huang, X.-C.; Lin, Y.-Y.; Zhang, J.-P.; Chen, X.-M. *Angew. Chem., Int. Ed.* **2006**, *45*, 1557. (c) Park, K. S.; Ni, Z.; Cote, A. P.; Choi, J. Y.; Huang, R.; Uribe-Romo, F. J.; Chae, H. K.; O'Keeffe, M.; Yaghi, O. M. *Proc. Natl. Acad. Sci. U.S.A.* **2006**, *103*, 10186. (d) Zhang, J.-P.; Zhu, A.-X.; Lin, R.-B.; Qi, X.-L.; Chen, X.-M. *Adv. Mater.* **2011**, *23*, 1268.
(10) Gücüyener, C.; van den Bergh, J.; Gascon, J.; Kapteijn, F. *J. Am. Chem. Soc.* **2010**, *132*, 17704.
(11) (a) Chang, N.; Gu, Z.-Y.; Yan, X.-P. *J. Am. Chem. Soc.* **2010**, *132*, 13645. (b) van den Bergh, J.; Gücüyener, C.; Pidko, E. A.; Hensen, E. J. M.; Gascon, J.; Kapteijn, F. *Chem.—Eur. J.* **2011**, *17*, 8832. (c) Karagiaridi, O.; Lalonde, M. B.; Bury, W.; Sarjeant, A. A.; Farha, O. K.; Hupp, J. T. *J. Am. Chem. Soc.* **2012**, *134*, 18790.
(12) Zhu, A.-X.; Lin, R.-B.; Qi, X.-L.; Liu, Y.; Lin, Y.-Y.; Zhang, J.-P.; Chen, X.-M. *Microporous Mesoporous Mater.* **2012**, *157*, 42.
(13) Zhang, J.-Y.; Cheng, A.-L.; Yue, Q.; Sun, W.-W.; Gao, E.-Q. *Chem. Commun.* **2008**, 847.
(14) (a) Banerjee, R.; Phan, A.; Wang, B.; Knobler, C.; Furukawa, H.; O'Keeffe, M.; Yaghi, O. M. *Science* **2008**, *319*, 939. (b) Wu, T.; Zhang, J.; Zhou, C.; Wang, L.; Bu, X.; Feng, P. *J. Am. Chem. Soc.* **2009**, *131*, 6111. (c) Tian, Y.-Q.; Yao, S.-Y.; Gu, D.; Cui, K.-H.; Guo, D.-W.; Zhang, G.; Chen, Z.-X.; Zhao, D.-Y. *Chem.—Eur. J.* **2010**, *16*, 1137.
(15) Beldon, P. J.; Fábián, L.; Stein, R. S.; Thirumurugan, A.; Cheetham, A. K.; Friščić, T. *Angew. Chem., Int. Ed.* **2010**, *49*, 9640.
(16) (a) Moulton, B.; Zaworotko, M. J. *Chem. Rev.* **2001**, *101*, 1629. (b) Zhang, J.-P.; Huang, X.-C.; Chen, X.-M. *Chem. Soc. Rev.* **2009**, *38*, 2385. (c) Elsaidi, S. K.; Mohamed, M. H.; Wojtas, L.; Chanthapally, A.; Pham, T.; Space, B.; Vittal, J. J.; Zaworotko, M. J. *J. Am. Chem. Soc.* **2014**, *136*, 5072.
(17) (a) Burtch, N. C.; Jasuja, H.; Walton, K. S. *Chem. Rev.* **2014**, *114*, 10575. (b) Devic, T.; Serre, C. *Chem. Soc. Rev.* **2014**, *43*, 6097.
(18) Zhang, K.; Lively, R. P.; Dose, M. E.; Brown, A. J.; Zhang, C.; Chung, J.; Nair, S.; Koros, W. J.; Chance, R. R. *Chem. Commun.* **2013**, *49*, 3245.
(19) (a) He, Y.; Krishna, R.; Chen, B. *Energy Environ. Sci.* **2012**, *5*, 9107. (b) Krishna, R. *Microporous Mesoporous Mater.* **2014**, *185*, 30.
(20) Cousin Saint Remi, J.; Baron, G. V.; Denayer, J. F. M. *J. Phys. Chem. C* **2013**, *117*, 9758.
(21) Liu, X.; Li, Y.; Ban, Y.; Peng, Y.; Jin, H.; Bux, H.; Xu, L.; Caro, J.; Yang, W. *Chem. Commun.* **2013**, *49*, 9140.
(22) Li, Z.; Zeng, H. C. *Chem. Mater.* **2013**, *25*, 1761.
(23) (a) Chizallet, C.; Lazare, S.; Bazer-Bachi, D.; Bonnier, F.; Lecocq, V.; Soyer, E.; Quoineaud, A.-A.; Bats, N. *J. Am. Chem. Soc.* **2010**, *132*, 12365. (b) Chizallet, C.; Bats, N. *J. Phys. Chem. Lett.* **2010**, *1*, 349.
(24) (a) Chang, N.; Yan, X.-P. *J. Chromatogr. A* **2012**, *1257*, 116. (b) Herm, Z. R.; Wiers, B. M.; Mason, J. A.; van Baten, J. M.; Hudson, M. R.; Zajdel, P.; Brown, C. M.; Masciocchi, N.; Krishna, R.; Long, J. R. *Science* **2013**, *340*, 960. (c) Kewley, A.; Stephenson, A.; Chen, L.; Briggs, M. E.; Hasell, T.; Cooper, A. I. *Chem. Mater.* **2015**, *27*, 3207.
(25) (a) Górna-Binkul, A.; Keymeulen, R.; Langenhove, H. V.; Buszewski, B. *J. Chromatogr. A* **1996**, *734*, 297. (b) Lin, G.-C.; Chang, C. A. *J. Chromatogr.* **1987**, *409*, 371.
(26) (a) Hattori, H.; Iwai, M.; Kurono, S.; Yamada, T.; Watanabe-Suzuki, K.; Ishii, A.; Seno, H.; Suzuki, O. *J. Chromatogr. B* **1998**, *718*, 285. (b) Joos, P. E.; Godoi, A. F. L.; De Jong, R.; de Zeeuw, J.; Van Grieken, R. *J. Chromatogr. A* **2003**, *985*, 191.
(27) Münch, A. S.; Mertens, F. O. R. L. *J. Mater. Chem.* **2012**, *22*, 10228.
(28) Gu, Z.-Y.; Yan, X.-P. *Angew. Chem., Int. Ed.* **2010**, *49*, 1477.
(29) Alaerts, L.; Kirschhock, C. E. A.; Maes, M.; van der Veen, M. A.; Finsy, V.; Depla, A.; Martens, J. A.; Baron, G. V.; Jacobs, P. A.; Denayer, J. F. M.; De Vos, D. E. *Angew. Chem., Int. Ed.* **2007**, *46*, 4293.
(30) (a) Yang, C.-X.; Yan, X.-P. *Anal. Chem.* **2011**, *83*, 7144. (b) Couck, S.; Rémy, T.; Baron, G. V.; Gascon, J.; Kapteijn, F.; Denayer, J. F. M. *Phys. Chem. Chem. Phys.* **2010**, *12*, 9413.

DOI: 10.1021/jacs.5b03727
J. Am. Chem. Soc. 2015, 137, 7217−7223

Supporting Information

Exceptional hydrophobicity of a large-pore metal-organic zeolite

Chun-Ting He,[†] Lu Jiang,[†] Zi-Ming Ye,[†] Rajamani Krishna,[‡] Zhen-Song Zhong,[†] Pei-Qin Liao,[†] Jianqiao Xu,[†] Gangfeng Ouyang,[†] Jie-Peng Zhang[†] and Xiao-Ming Chen[†]*

[†] MOE Key Laboratory of Bioinorganic and Synthetic Chemistry, School of Chemistry and Chemical Engineering, Sun Yat-Sen University, Guangzhou 510275, China

[‡] Van't Hoff Institute for Molecular Sciences, University of Amsterdam, Science Park 904, 1098 XH Amsterdam, The Netherlands

*E-mail: zhangjp7@mail.sysu.edu.cn

Supplementary Index

Experimental Section

1. Materials

Commercially available reagents, including 2-ethylimidazole, $Zn(OH)_2$, and concentrated aqueous ammonia (25%), were used as received without further purification.

2. Instrumentations

Thermogravimetry analyses were performed at a rate of 10 ^oC/min under N_2 using a TA Q50 system. Powder X-ray diffraction (PXRD) data were recorded on a Rigaku D-MAX 2200 VPC or a Bruker D8 Advance diffractometer (Cu Kα) at room temperature. Vapor sorption isotherms were measured on a BELSORP-max volumetric adsorption apparatus. The sorption isotherms for N_2 was measured with an automatic volumetric sorption apparatus Micromertics ASAP 2020M. Before each sorption experiment, the sample was heated at 100 ^oC under high vacuum for 5 h to remove the remnant solvent molecules. Ultra-high-purity (99.999%) N_2 and analytical reagents (methanol, ethanol and benzene) were used for measurements. The temperatures were controlled by a liquid-nitrogen bath (77 K) or a water bath (298 K). Langmuir surface area and the pore volume were calculated by the saturated uptake using Langmuir fitting. Gas chromatography (GC) experiments were performed on an Agilent 7890A system with a thermal conductivity detector (TCD). The data acquisition and processing were controlled by the ChemStation software. The inlet temperature of the gas chromatograph and the temperature of TCD were set to 250 ^oC. Nitrogen (99.999%) was used as the carrier gas. For each GC injection, 5 μL aliquot of analytes was first introduced to a N_2-filled, 25-mL gastight glass vial and heated at 100 ^oC for 3 min, then an analyte-N_2 mixture (20 μL for xylene isomers, benzene/cyclohexene/cyclohexane, and styrene/ethylbenzene, 4 μL of C6 alkane isomers and 6 μL of C6-C10 linear alkanes) was injected. The water contact angles were measured on the contact angle system OCA 20 (Dataphysics, Germany).

3. Synthesis

All synthetic experiments were carried out at room temperature using a rapid solution mixing method using a methanol solution of 2-ethylimidazole (4 mmol) and a

concentrated aqueous ammonia (25%) solution of $Zn(OH)_2$ (2 mmol) as reactants. The reaction was carried out by fast dropping one reactant solution into another (in ca. 4-5 min). Benzene or cyclohexane was premixed with the latter reactant solution before the reaction, unless otherwise stated. The resultant slurry was stirred at room temperature for 0.5 h, and then filtered, washed by methanol, and dried at 120 ^oC in air to give white microcrystalline powder as the product.

Synthetic procedures for samples used for property characterization:

MAF-4: Synthesized according to a published procedure,[s1] which is similar for MAF-5.

MAF-5: A methanol (6 mL) solution of Heim (4 mmol, 0.384 g) was fast added (in 4-5 min) into a concentrated aqueous ammonia solution (25%, 40 mL) of $Zn(OH)_2$ (2 mmol, 0.198 g) premixed with cyclohexane (3.25%, v/v). Yield ca. 0.45 g (88%).

MAF-6: A concentrated aqueous ammonia solution (25%, 40 mL) of $Zn(OH)_2$ (2 mmol) was added into a methanol (30 mL) solution of Heim (4 mmol, 0.38 g) premixed with cyclohexane (6.66%, v/v). Yield ca. 0.40 g (78%).

4. Fabrication of the GC capillary column

MAF-6 was dispersed in methanol under sonication and let sit for 12 h, and then the colloid suspension on the upper layer was collected by centrifugation and washed with fresh methanol, and dried at 120 °C in air. Before coating MAF-6, the fused silica capillary (15 m long × 0.53 mm i.d.; i.d. = internal diameter) was washed sequentially by NaOH (2 mol/L) for three times (and then immersed for 3 h), ultrapure water (until the pH of outflow reached 7.0), HCl (1 mol/L) for three times (and then immersed for 1 h), ultrapure water (until the pH of outflow reached 7.0), methanol for three times, and then dried by a nitrogen purge at 120 ^oC for 3 h. MAF-6 was coated onto the pre-treated capillary column by a dynamic coating method. A methanol suspension of MAF-6 (10 mg in 1.0 mL) was pushed through the column by a nitrogen flow (inlet pressure: 0.4 MPa) to leave a wet coating layer (ca. 0.1 mL) on the inner wall of the capillary column. After coating, the capillary column was settled for 1 h for conditioning under nitrogen flow. Further conditioning of the capillary column was carried out using a temperature program:

60 °C for 30 min, then 5 °C min^{-1} to 150 °C and 150 °C for 60 min, then 5 °C min^{-1} to 250 °C and 250 °C for 60 min. The temperature program was repeated for 3 times.

5. Program of GC separation

Chromatograms for GC separation of linear alkanes (100 ng each) used a temperature program: 80 °C for 1 min, then 20 °C min^{-1} to 200 °C at a N_2 flow rate of 6 mL min^{-1}; for hexane and its branched isomers (100 ng each): 55 °C for 1.5 min, then 10 °C min^{-1} to 100 °C at a N_2 flow rate of 5 mL min^{-1}; for xylene isomers (1000 ng each): kept the temperature at 100 °C under a N_2 flow rate of 5 mL min^{-1}; for styrene and ethylbenzene (1500 ng each): kept the temperature at 120 °C under a N_2 flow rate of 5 mL min^{-1}; for benzene, cyclohexene and cyclohexane (1000 ng each): kept the temperature at 80 °C under a N_2 flow rate of 5 mL min^{-1}.

6. Calculation of selectivity factors, resolution and thermodynamic parameters

The selectivity factors for analytes A and B on the capillary column were calculated from the gas chromatogram according to

$$\alpha_{B/A} = \frac{t_B - t_0}{t_A - t_0}$$

where t_A, t_B, and t_0 are the retention times of analytes A and B, as well as the reference nitrogen carrier gas (i.e. the column void time), respectively, under the same operation conditions.

The resolution for analytes A and B on the capillary column were calculated from the gas chromatogram according to

$$R = \frac{t_B - t_A}{1/2(w_B + w_A)}$$

where t_A and t_B are the retention times of analytes A and B, and w_A and w_B are the peak widths of analytes A and B, respectively.

The enthalpy change (ΔH) and entropy change (ΔS) for the transfer of solutes from the

mobile phase to the stationary phase were calculated from the van't Hoff equation

$$\ln k' = \frac{-\Delta H}{RT} + \frac{\Delta S}{R} + \ln \Phi$$

Where k' is the retention factor, R is the gas constant, T is the absolute temperature, and ϕ is the phase ratio.

k' is calculated by

$$k' = \frac{t - t_0}{t_0}$$

where t and t_0 are the retention times for the analyte and nitrogen carrier gas (i.e. the column void time), respectively, under the same operation conditions.

ϕ was calculated by

$$\Phi = \frac{v_s}{v_0}$$

Where V_S is the volume of the stationary phase in the column, and V_0 is the void volume of the column. In this work V_0 was 3.31 cm^3 (= 3.14 × (0.053/2 cm)^2 × 1500 cm), V_S was 1.13 × 10^{-3} cm^3 (= 1.0 × 10^{-3} g/0.885 g cm^{-3}). Thus, $\ln \Phi$ was estimated to be -7.98.

7. Molecular dynamic (MD) simulations

Molecular dynamic (MD) simulations were performed by the MS 5.0 modeling package. Firstly, we cleaved the MAF crystal on specific crystal surfaces according to their crystal morphologies, after which the unsaturated metal ions were terminated by hydroxyl groups. These structural models were energy-minimized maintaining fixed the metal atomic coordinates. Then, a layer of water molecules (thickness of 15 Å) with density of 1.0 g cm^{-3} was put onto each target crystal surface and the structure of the water-crystal surface system was simulated by MD with the constant volume/constant temperature (NVT) ensemble. All the calculations employed the Dreiding forcefield and the QEq partial charges were adopted for the atoms of the surfaces while ESP charges were adopted for water molecules (-0.706e and 0.353e for O and H atoms, respectively, where e =

1.6022×10^{-19} C is the elementary charge). Nose thermostat and random initial velocities were used and the electrostatic as well as the van der Waals interactions were evaluated by the Ewald summation method, while all the Buffer widths were set as 0.5 Å. The timestep was 1 fs and the total simulation time was 500 ps with the dynamic temperature chosen as 298 K.

8. Fitting of pure component isotherms and simulation methodology for transient breakthrough.

The experimentally measured loadings of water, methanol, ethanol, and benzene in MAF-6 obtained at room temperature, i.e. 298 K, were fitted with the dual-site Langmuir-Freundlich model

$$q = q_{A,sat}\frac{b_A p^{\nu_A}}{1+b_A p^{\nu_A}} + q_{B,sat}\frac{b_B p^{\nu_B}}{1+b_B p^{\nu_B}}$$

The Langmuir-Freundlich parameters are provided in Table S5. Figure S6 provides a comparison of the pure component isotherm data with dual-site Langmuir-Freundlich fits. The isotherms of all guest adsorbates water, methanol, ethanol, and benzene exhibit steep increases. In order to properly capture the steep isotherms, the Freundlich exponents need to have large values in the range of 5-10.

The transient breakthrough simulations in a fixed bed adsorber packed with MAF-6 is schematized in Figure S7. The methodology used in the transient breakthrough simulations is discussed in detail in the earlier work.[s2] For presenting the breakthrough simulation results, we use the dimensionless time, $\tau = \frac{tu}{L\varepsilon}$, obtained by dividing the actual time, t, by the characteristic time, $\frac{L\varepsilon}{u}$, where L is the length of adsorber, u is the superficial fluid velocity, ε is the bed voidage.[s3] Intra-crystalline diffusion effects are characterized by the parameter $\frac{Đ_i}{r_c^2}$, where r_c is the radius of the crystallites, and $Đ_i$ is the Maxwell-Stefan diffusivity. In the breakthrough simulations, the chosen values of $\frac{Đ_i}{r_c^2}$ were guided by available experimental data.[s4-7] If the values of $\frac{Đ_i}{r_c^2}$ are large enough,

then the intra-crystalline diffusion effects are of negligible importance. For all the simulations reported in this article we choose L = 0.3 m; u = 0.04 m s^{-1}; and ε = 0.4. Moreover, intra-crystalline diffusion effects are considered to be of negligible importance. The transient uptake data for mesitylene in Figure S8 strongly suggests that intra-crystalline diffusion resistances are unlikely to be significant in MAF-6.

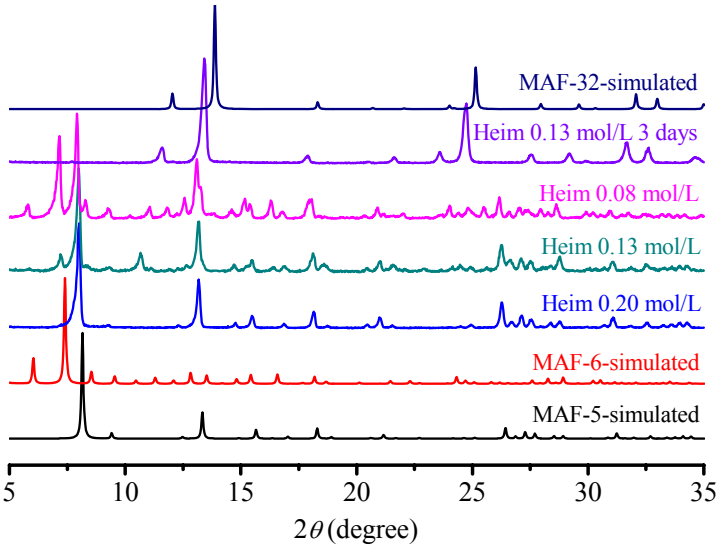

Figure S1. PXRD patterns of the products obtained by adding a concentrated aqueous ammonia solution of $Zn(OH)_2$ into a methanol solution of Heim without template.

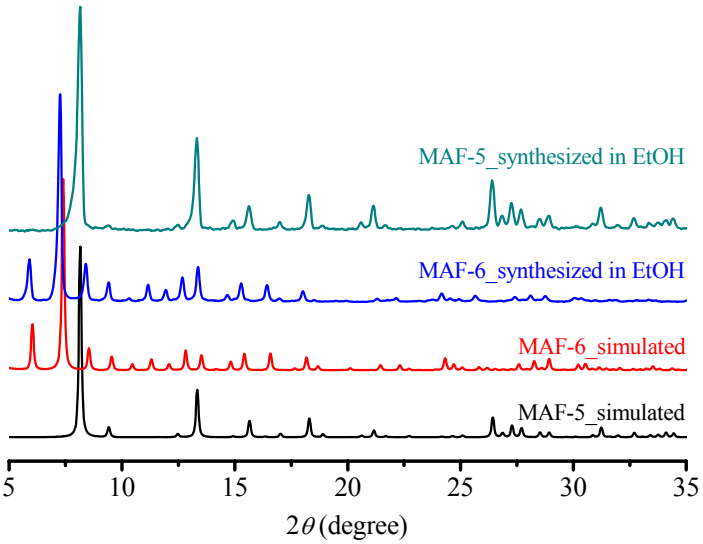

Figure S2. PXRD patterns of MAF-6 synthesized by adding a concentrated aqueous ammonia solution of $Zn(OH)_2$ into ethanol solution of Heim (concentration 0.08-0.13 mol/L) premixed with template (6.66%, v/v) and MAF-5 synthesized by adding a ethanol solution of Heim into a concentrated aqueous ammonia solution of $Zn(OH)_2$ premixed with template (3.25%, v/v).

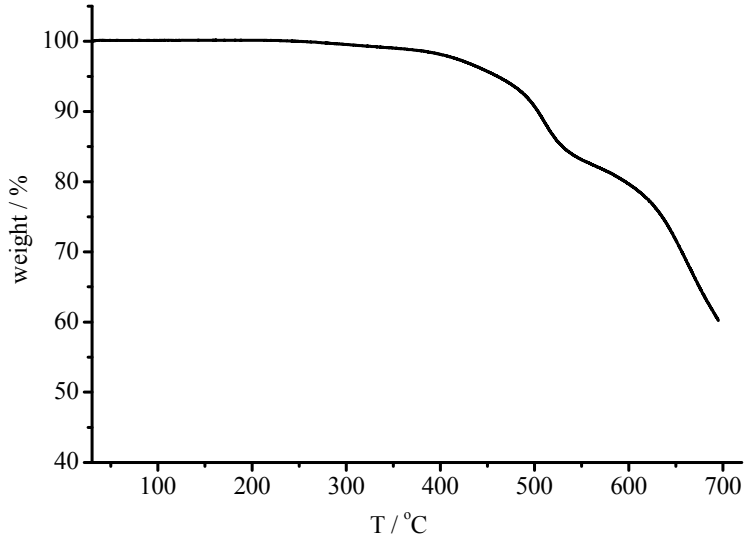

Figure S3. Thermogravimetry curve of MAF-6.

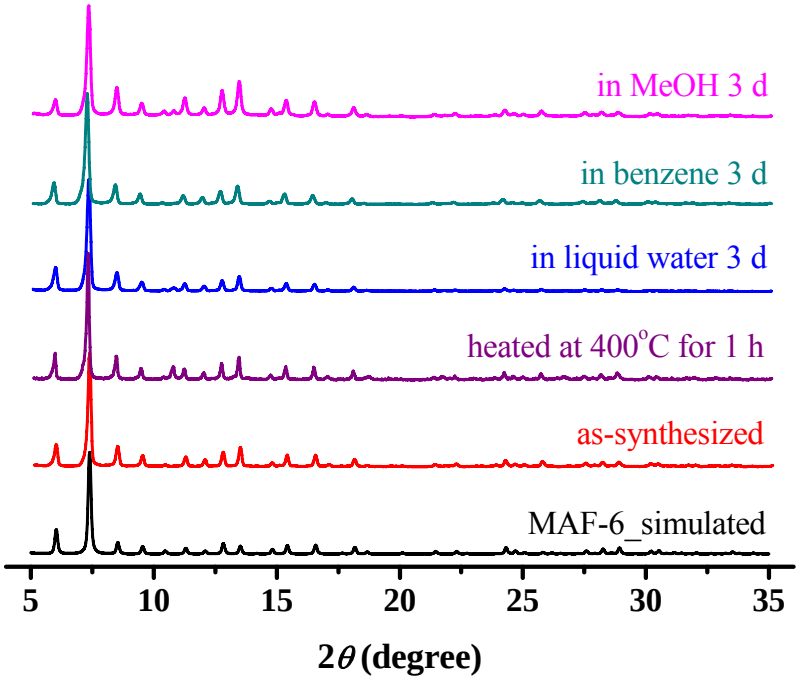

Figure S4. PXRD patterns of MAF-6 after different thermal/chemical treatments.

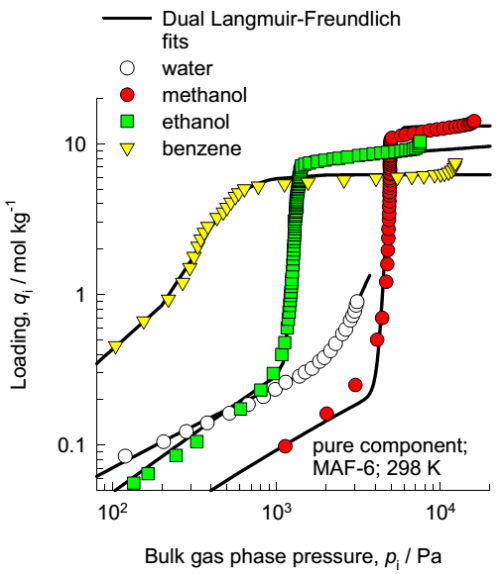

Figure S5. Comparison of the pure component isotherm data with dual-site Langmuir-Freundlich fits (parameters as provided in Table S5) or adsorption of water, methanol, ethanol, and benzene in MAF-6 obtained at 298 K.

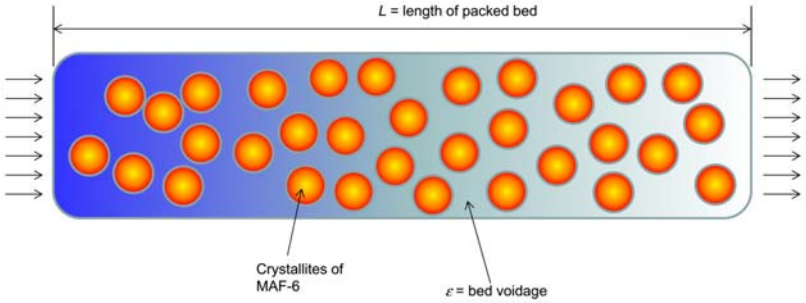

Figure S6. Schematic of a packed bed adsorber.

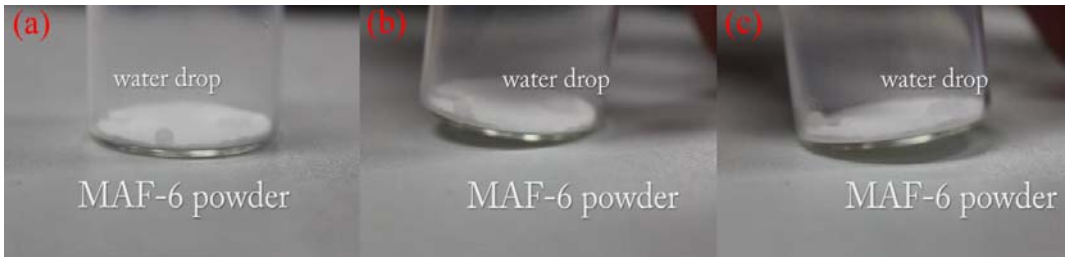

Figure S7. Snapshots of water droplet maintaining its shape (a) and rolling (b and c) on the powders of MAF-6. See supplementary movie for detail.

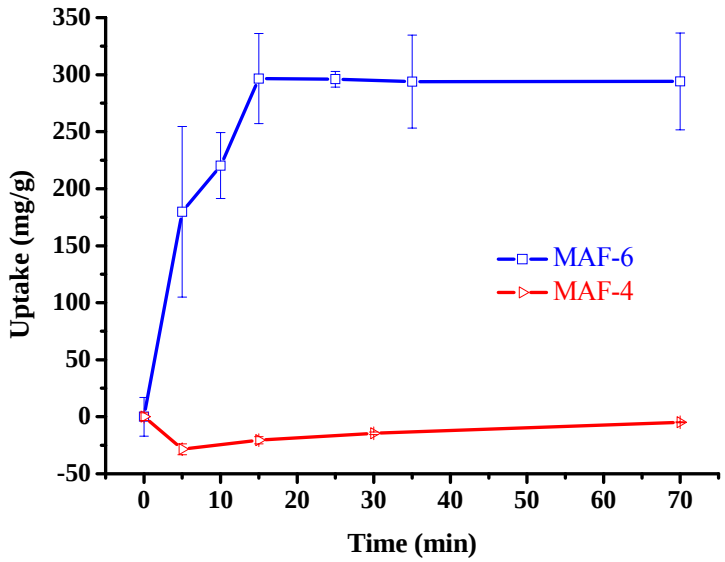

Figure S8. Mesitylene adsorption kinetics of MAF-4 and MAF-6 (The error bar shows the standard deviation of three repeated measurements).

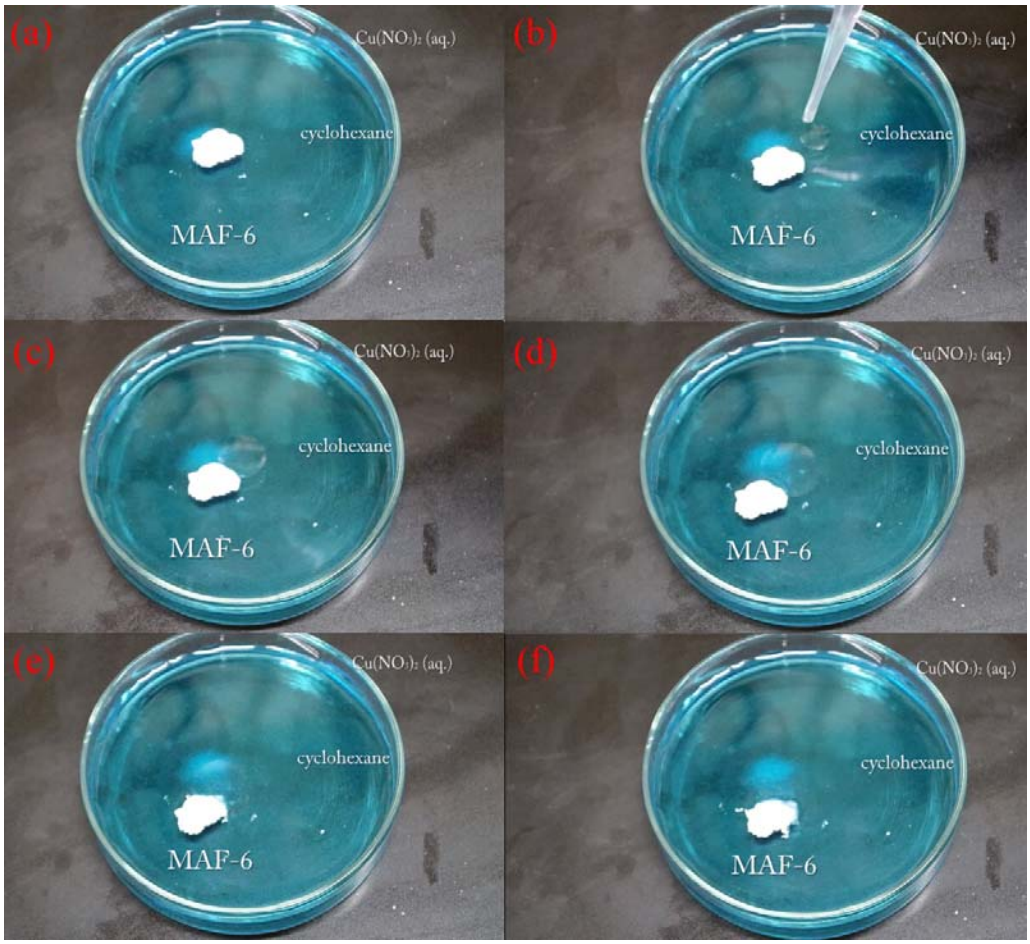

Figure S9. Snapshots of the process for cyclohexane adsorbed by MAF-6 powders on the surface of water (for clearly, water was colored by $Cu(NO_3)_2$). (a-f) t = 0, 3, 5, 10, 15 20 s. See supplementary movie for detail.

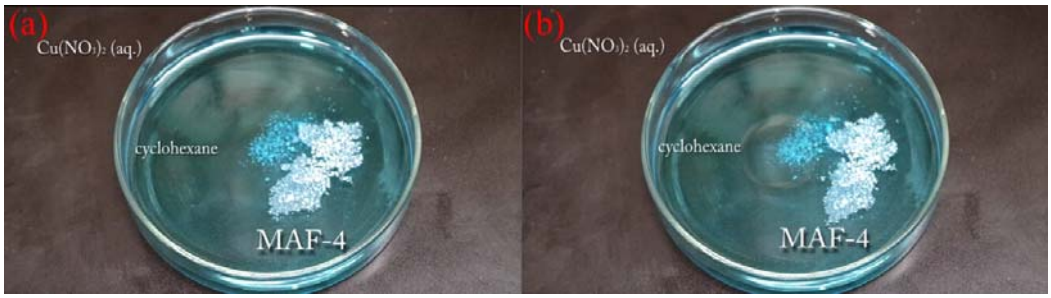

Figure S10. Snapshots before (a) and 3 min after (b) cyclohexane added on the side of MAF-4 powders. See supplementary movie for detail.

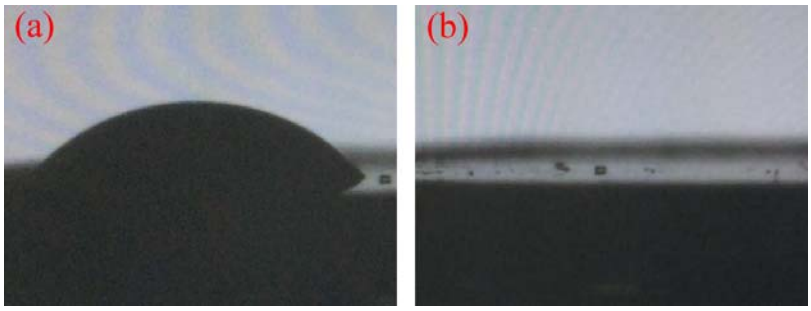

Figure S11. Contact angle images of water droplet on MAF-4 powders for 1 s (a) and 40 s (b). See supplementary movie for detail.

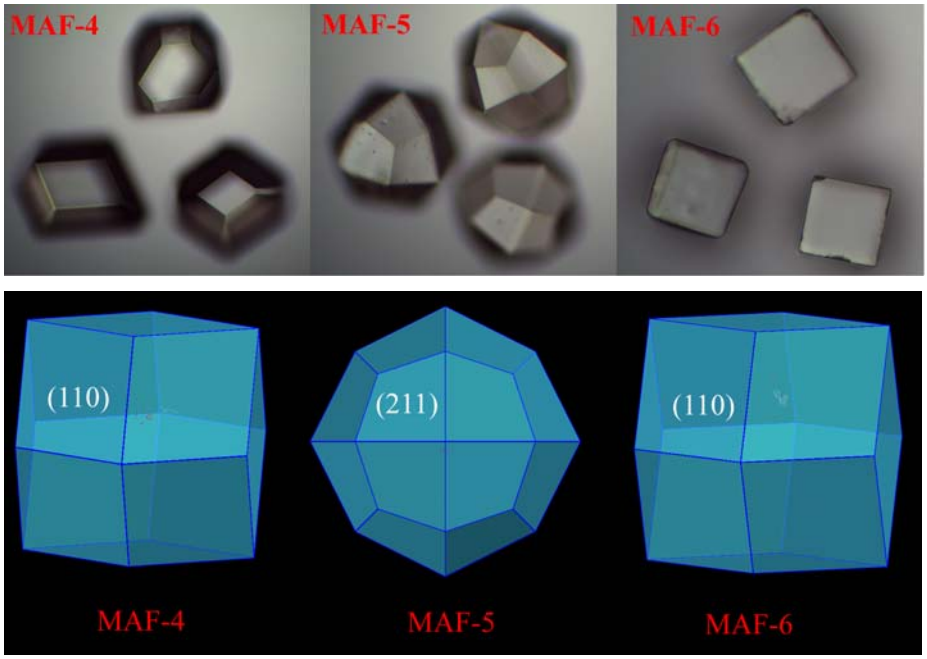

Figure S12. Experimental (top) and Bravais–Friedel–Donnay–Harker (BFDH) (bottom) crystal morphologies of MAF-4, MAF-5 and MAF-6. (Note: The theoretical favourite crystal surfaces of MAF-4 ([110]), MAF-5 ([211]) and MAF-6 ([110]) are not completely the same with the experimental ones ([100] and [110] for MAF-4, [100] and [211] for MAF-5, [100] for MAF-6). So, our MD modelling is finally based on the experimental crystal morphologies.)

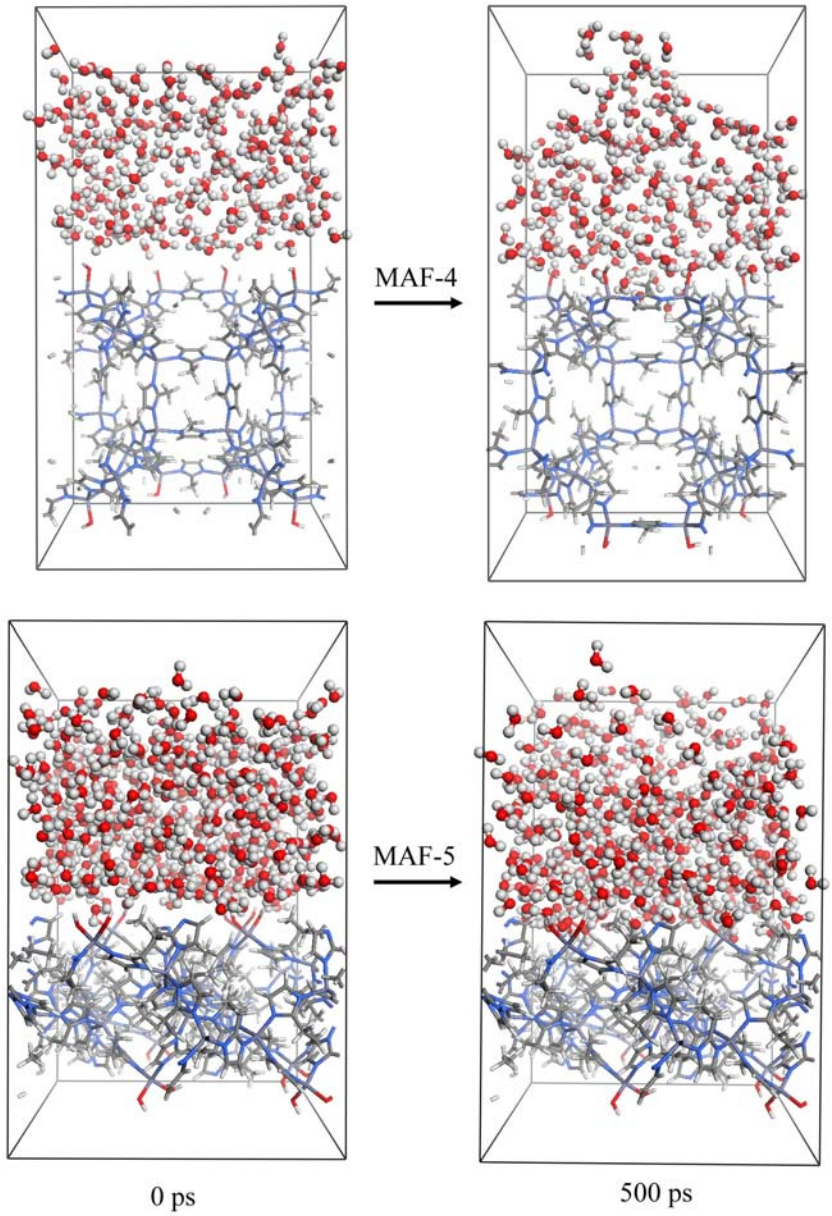

Figure S13. Snapshots of water-crystal surface systems for the (110) and (211) crystal surfaces of MAF-4 and MAF-5, respectively, obtained from the MD simulations (left: initial configurations at 0 ps; right: optimized configurations after 500 ps).

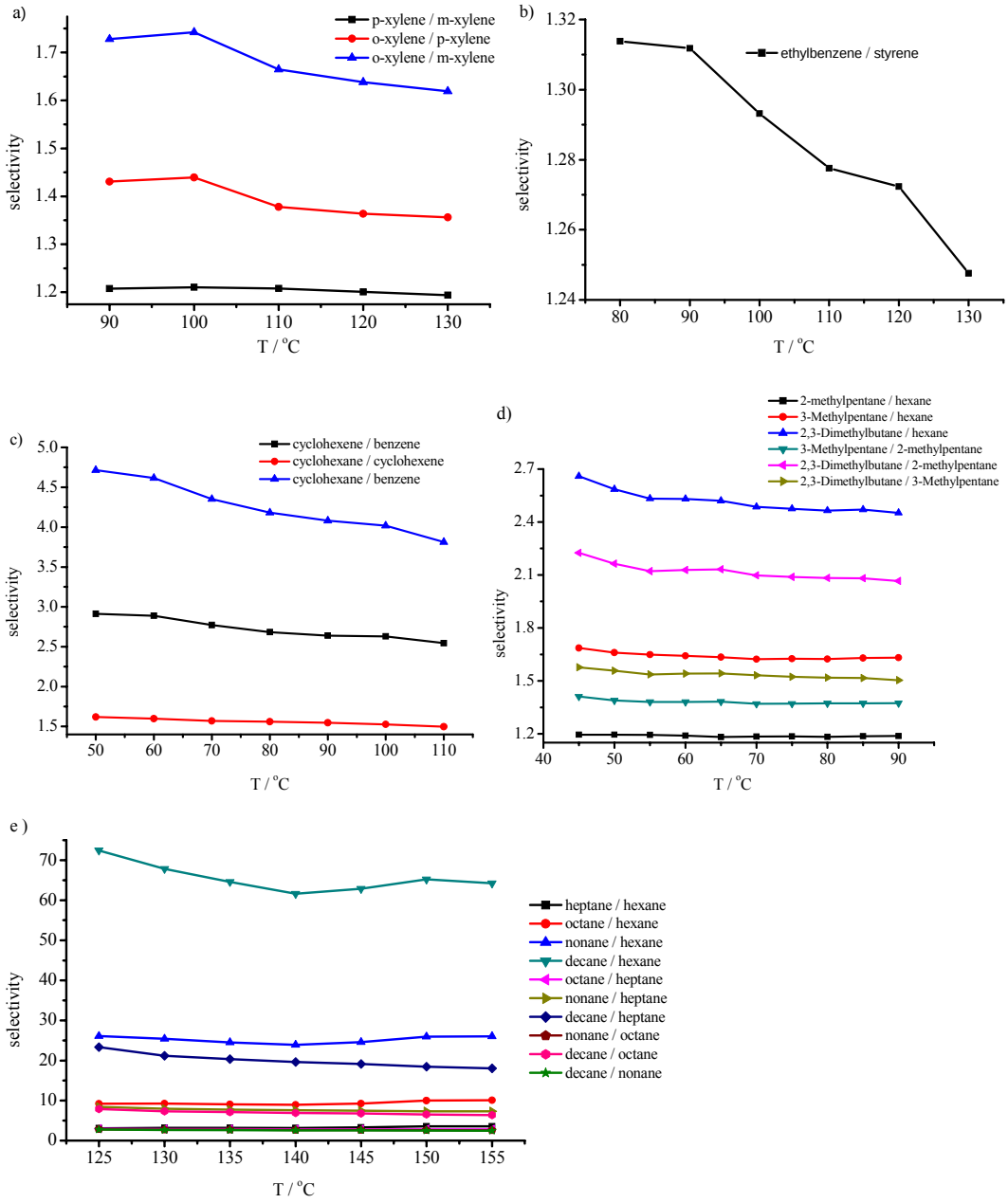

Figure S14. Effect of temperature on the selectivity for the separation of alkanes and benzene homologues on the MAF-6 coated capillary column.

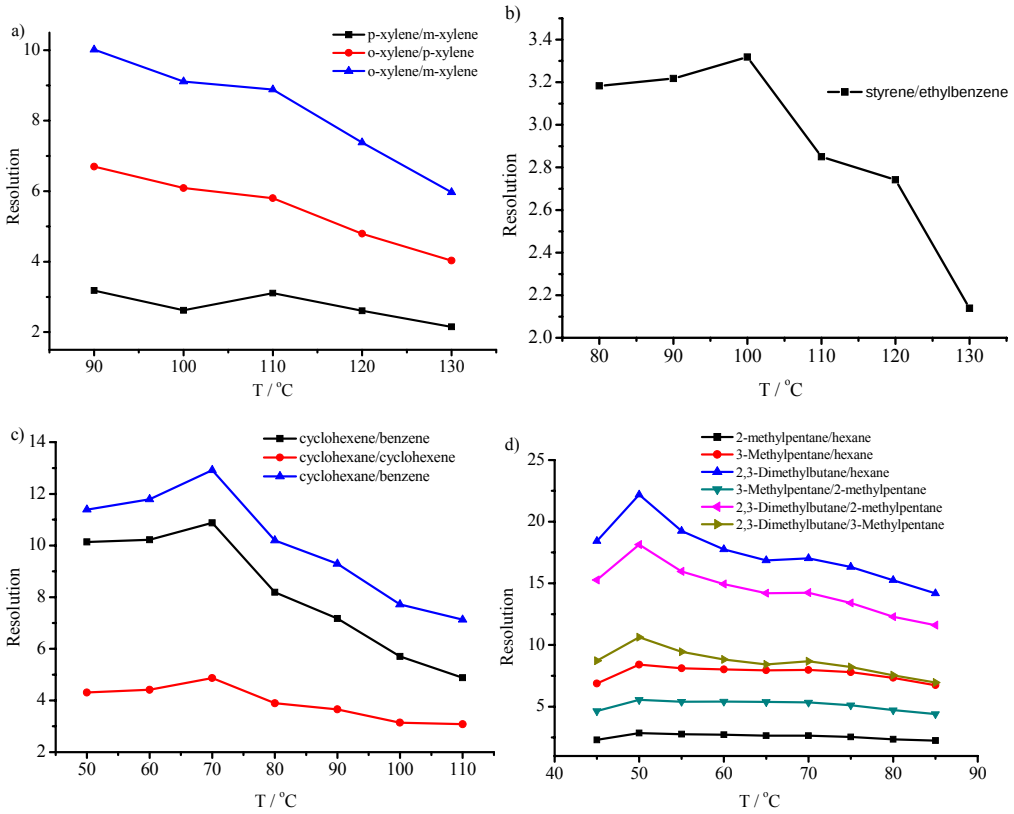

Figure S15. Effect of temperature on the resolution for the separation of alkanes and benzene homologues on the MAF-6 coated capillary column.

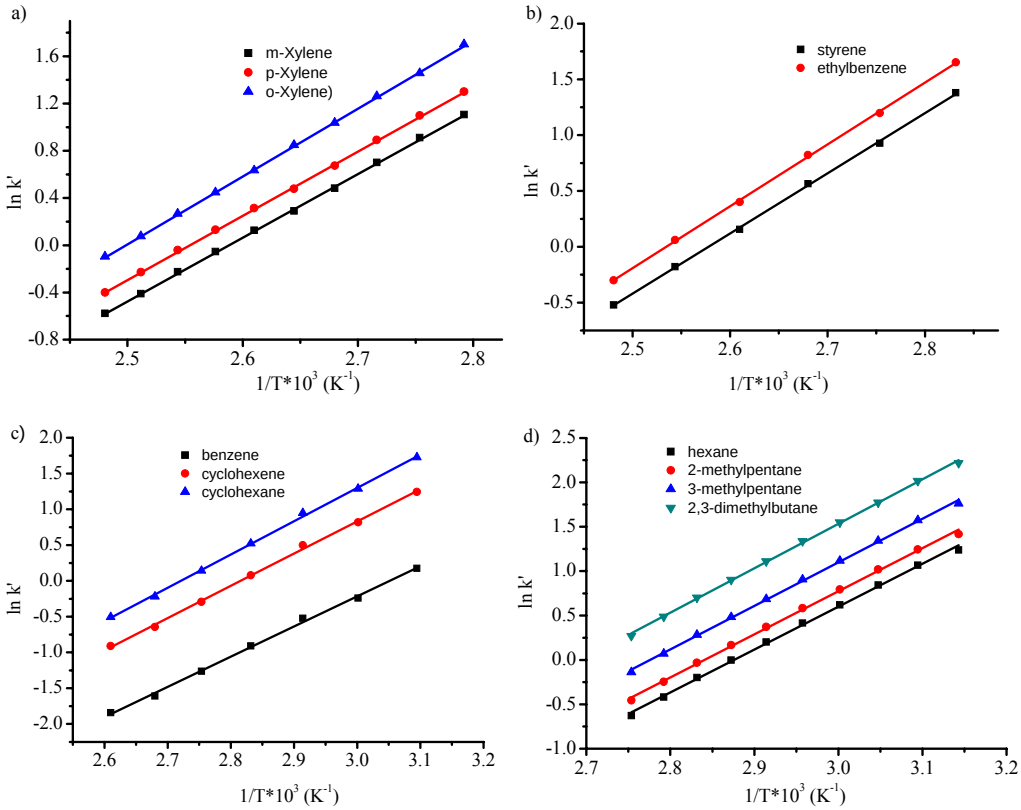

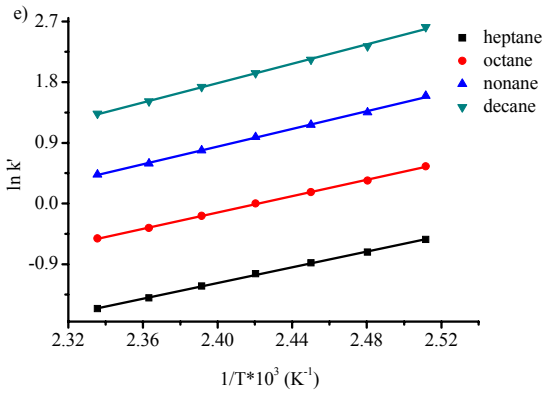

Figure S16. van't Hoff plots (variation in capacity factor *k′* with temperature *T*) for the MAF-6 coated capillary column.

Table S1 Selected crystallography structural characteristics of four representative zeolitic MAFs.

	Composition	Topology	Void (%)	Crystal density (g cm^{-3})	Pore volume (cm^3 g^{-1})	Cavity size (Å)	Aperture size (Å)
MAF-3	Zn(II) benzimidazolate	SOD	26.6	1.241	0.21	6.3 × 4.1	2.9
MAF-4	Zn(II) 2-methylimidazolate	SOD	47.0	0.914	0.51	12.5	3.2
MAF-5	Zn(II) 2-ethylimidazolate	ANA	32.8	1.083	0.30	7.0 × 10.0	4.0 × 5.8
MAF-6	Zn(II) 2-ethylimidazolate	RHO	55.4	0.885	0.63	18.1	7.6

NOTE: The Framework Densities (FD_{Si}) of prototypical SOD, ANA, and RHO SiO_2 based zeolites are 16.7, 19.2, and 14.5 T/1000 $Å^3$, respectively, which represent the pore volume differences of these metal-organic zeolites and corresponding inorganic zeolites. MAF-3 possesses a compressed SOD topology crystallizes in the trigonal system, as well as a much bulkier side group, which significantly reduces its porosity.

Table S2. Precision for separations of benzene homologues and alkane isomers on the MAF-6 coated capillary column.

Analytes	RSD (%) (n =5)		
	t	$W_{1/2}$	Peak area
m-Xylene	0.19	2.28	3.30
p-Xylene	0.14	0.87	4.28
o-Xylene	0.14	0.54	1.54
Styrene	0.50	5.86	4.46
Ethylbenzene	0.55	7.45	5.76
Benzene	0.58	＜0.01	5.72
Cyclohexene	0.24	0.73	3.93
Cyclohexane	0.24	0.64	3.40
Hexane	0.23	0.44	1.83
2-Methylpentane	0.21	1.36	2.09
3-Methylpentane	0.18	0.94	1.65
2,3-Dimethylbutane	0.10	3.22	6.66
Heptane	0.20	6.50	7.33
Octane	0.07	2.67	6.62
Nonane	0.09	1.67	4.41
Decane	0.08	7.34	5.19

Table S3 Comparison of some general parameters between the saturated/unsaturated analogues mentioned in this work

	Benzene	Cyclohexene	Cyclohexane	Styrene	Ethylbenzene
Retention time /min	1.57	2.45	2.94	0.99	1.11
Boiling point/^{o}C	80	83	81	145	136
log $P_{oct/wat}$	2.177±0.154	2.918±0.188	3.613±0.158	2.821±0.191	3.229±0.169
Dielectric constant ε	2.283	2.218	2.020	2.47	2.446

Table S4. Experimental thermodynamic parameters for GC separation of alkane isomers and benzene homologues on the MAF-6 column.

Analytes	Boiling point (°C)	ΔH (kJ mol^{-1})	ΔS (J mol^{-1} K^{-1})
m-Xylene	139	-44.83 ± 0.04	-49.70 ± 0.09
p-Xylene	138	-45.23 ± 0.03	-49.19 ± 0.09
o-Xylene	144	-47.75 ± 0.03	-52.98 ± 0.07
Styrene	145	-44.82 ± 0.06	-49.19 ± 0.15
Ethylbenzene	136	-46.04 ± 0.05	-50.33 ± 0.14
Benzene	80	-35.08 ± 0.09	-40.67 ± 0.25
Cyclohexene	83	-37.44 ± 0.07	-39.07 ± 0.21
Cyclohexane	81	-38.68 ± 0.07	-38.90 ± 0.19
2-Methylpentane	60	-40.34 ± 0.06	-48.26 ± 0.19
3-Methylpentane	63	-40.80 ± 0.05	-46.94 ± 0.15
2,3-Dimethylbutane	58	-41.65 ± 0.05	-45.86 ± 0.14
Hexane	69	-40.15 ± 0.07	-49.13 ± 0.20
Heptane	99	-48.40 ± 0.07	-59.60 ± 0.17
Octane	126	-50.33 ± 0.06	-55.55 ± 0.14
Nonane	150	-54.56 ± 0.09	-57.57 ± 0.23
Decane	174	-59.65 ± 0.13	-61.97 ± 0.32

Table S5. Dual-site Langmuir-Freundlich parameters for adsorption of water, methanol, ethanol, and benzene at 298 K in MAF-6. These fits are for the "adsorption" branch of the isotherms.

Adsorbate	Site A			Site B		
	$q_{A,sat}$ mol kg^{-1}	b_{A0} Pa$^{-\nu_A}$	ν_A dimensionless	$q_{B,sat}$ mol kg^{-1}	b_{B0} Pa$^{-\nu_B}$	ν_B dimensionless
water	2	4.25×10^{-20}	5.4	2	3.24×10^{-3}	0.54
methanol	1	7.07×10^{-4}	0.72	12.7	2.11×10^{-89}	24
ethanol	4	3.09×10^{-4}	0.8	7.8	1.87×10^{-84}	26.8
benzene	0.54	2.77×10^{-5}	2.5	5.7	9.51×10^{-10}	3.4

References

(1) A.-X. Zhu, R.-B. Lin, X.-L. Qi, Y. Liu, Y.-Y. Lin, J.-P. Zhang and X.-M. Chen, *Microporous and Mesoporous Materials*, 2012, **157**, 42-49.

(2) Krishna, R., *Microporous Mesoporous Mater*. 2014, **185**, 30-50.

(3) Krishna, R.; Long, J. R., *J. Phys. Chem. C* 2011, **115**, 12941-12950.

(4) Kärger, J.; Binder, T.; Chmelik, C.; Hibbe, F.; Krautscheid, H.; Krishna, R.; Weitkamp, J., *Nature Materials* 2014, **13**, 333-343.

(5) Zhang, K.; Lively, R. P.; Zhang, C.; Chance, R. R.; Koros, W. J.; Sholl, D. S.; Nair, S., *J. Phys. Chem. Lett.* 2013, **4**, 3618-3622.

(6) Zhang, K.; Lively, R. P.; Zhang, C.; Koros, W. J.; Chance, R. R., *J. Phys. Chem. C* 2013, **117**, 7214-7225.

(7) Zhang, K.; Lively, R. P.; Dose, M. E.; Brown, A. J.; Zhang, C.; Chung, J.; Nair, S.; Koros, W. J.; Chance, R. R., *Chem. Commun.* 2013, **49**, 3245-3247.